Polarimetric Detection and Range Estimation of a Point-Like Target

CHENGPENG HAO, Senior Member, IEEE
Chinese Academy of Sciences
Beijing, China

SAEED GAZOR, Senior Member, IEEE
Queens University
Ontario, Canada

XIAOCHUAN MA
SHEFENG YAN, Senior Member, IEEE
CHAOHUAN HOU, Fellow, IEEE
Chinese Academy of Sciences
Beijing, China

DANILO ORLANDO, Senior Member, IEEE
Università degli Studi "Niccolò Cusano"
Roma, Italy

In this paper, we deal with the problem of polarimetric diversity detection for point-like targets in the presence of Gaussian clutter with unknown covariance matrix. To this end, we jointly exploit the polarization diversity and the spillover of target energy to consecutive range samples to improve the performances of detection and range localization. For estimation purposes, we assume that a set of secondary data (free of signal components) is available with the same covariance matrix as the clutter in the cells under test. Because the uniformly most powerful test does not exist for this problem, we derive two adaptive detectors: the generalized likelihood ratio test and the Wald test. Interestingly, these new receivers ensure the constant false alarm rate property with respect to covariance matrix of the clutter. The performance assessments conducted on both simulated data and real recorded dataset reveal that the proposed detectors outperform, in both detection and localization, the traditional state-of-the-art counterparts that ignore either the polarimetry or the spillover.

Manuscript received September 2, 2014; revised March 17, 2015; released for publication July 10, 2015.

DOI. No. 10.1109/TAES.2015.140657.

Refereeing of this contribution was handled by R. Narayanan.

This work was supported by the National Natural Science Foundation of China under Grant Nos. 61172166 and 61222107.

Authors' addresses: C. Hao, X. Ma, S. Yan, C. Hou, Institute of Acoustics, Chinese Academy of Sciences, 100190 Beijing, China; S. Gazor, Department of Electrical and Computer Engineering, Queens University, K7L 3N6 Kingston, Ontario, Canada; D. Orlando, Università degli Studi "Niccolò Cusano," via Don Carlo Gnocchi 3, 00166 Roma, Italy, Corresponding author is S. Yan, E-mail: (sfyan@mail.ioa.ac.cn).

I. INTRODUCTION

Techniques for space-time adaptive detection in an unknown disturbance (i.e., clutter plus noise) environment stem from the pioneering work of Kelly [1], followed by Robey and colleagues seminal paper [2], and have received increasing attention in recent years in the radar community. In particular, Kelly [1], resorting to the generalized likelihood ratio test (GLRT), derives a constant false alarm rate (CFAR) test for detecting signals known up to a scaling factor, and Robey et al. [2] propose another CFAR test called adaptive matched filter (AMF) using the so-called two-step GLRT-based design procedure. Many recent solutions rely on such GLRT design procedures. For instance, these tests are extended versions for the distributed target, the multistatic radar, and the diagonal loading, respectively, in [3–5], and their Bayesian versions are introduced in [6]. More recently, in [7, 8], the authors apply both tests to derive receivers for detecting a double subspace signal. Other different solutions as an alternative to the GLRT can be found in the open literature (see, e.g., [9–18]).

Another important issue concerns the design assumptions of the nominal target. Specifically, all aforementioned detectors are based on the assumption that there is no spillover of the target energy to adjacent matched filter returns, i.e., they suppose that the target is exactly at the location corresponding to the sample time. This assumption is not reasonable because there is no guarantee that the samples of the matched filter output be exactly at the peak of the target return. The physical spillover phenomenon in a radar system happens as the centroid of the received target pulse is somewhere between two consecutive range bins [19, 20]. The spillover causes an important loss in radar signal processing, making all of the above detectors to suffer from this loss. As a remedy to this loss some works in open literature take into account this spillover. In [21, 22], the spillover information is exploited as a boon rather than a nuisance; by using two adjacent matched filter samples, they show that a monopulse radar might resolve up to five targets instead of two. In [23], this framework is extended to the context of space-time adaptive processing [24] for a single polarimetric channel, and two GLRT detectors are proposed. These detectors attempt to account for the spillover of target energy to enhance the target localization. In [25], the authors exploit additional structure of the clutter covariance matrix, i.e., the persymmetric property, to improve their robustness in training-limited scenarios [26, 27].

In this work, we move one step further and design space-time radar detectors that exploit the spillover of target energy and also use the polarization diversity to enhance the detection and range estimation performances. The polarization diversity is used in [28] and has been widely shown to enhance the radar detectors during the last decades both for military and civilian applications. Following [28], some adaptive detection schemes have

been proposed in [29–43] by explicitly taking into account the polarization diversity. For example, the detection of point-like targets embedded in Gaussian clutter with unknown spectral properties has been addressed in [29–31]. The detection of point-like and range-spread targets in compound-Gaussian clutter with unknown spectral properties has been considered in [32–35]. More recently, the polarization detection problem of multiple-input/multiple-output radar has been investigated in [37, 38]. Other recent solutions can be found in [39–43] and references therein.

We generalize the framework proposed in [23] to the polarimetric case. We first establish the discrete-time model of the received signal for two different polarimetric channels and then apply the plain GLRT and the Wald test to obtain two decision schemes because the uniformly most powerful (UMP) receiver does not exist for this problem. Interestingly, these detectors guarantee the CFAR property with respect to the unknown parameters of the clutter. Our performance assessment, carried out on simulated dataset and real dataset, shows that the exploitation of the polarization diversity can enhance the performances of detection and range estimation.

The remainder of the paper is organized as follows. The next section is devoted to the problem formulation. Section III focuses on the design of the detectors while Section IV provides illustrative examples. Section V contains some concluding remarks and hints for future work.

II. PROBLEM FORMULATION

In this section, we first describe a space-time spillover model for a single polarimetric channel and then extend it for two polarimetric channels. This is because the derivations and analysis are easier for two channels [33–35]. Moreover, real data are mostly available for two polarimetric channels. Our results can be extended to process the full polarimetric information [31, 32]. For a single polarimetric channel, the vector of the clutter returns representing the ith range cell is given by [44]

$$\mathbf{x}_i = \mathbf{s}_i + \mathbf{n}_i \in \mathbb{C}^{N\times 1}, \tag{1}$$

where $N = N_a\, N_p$, N_a is the number of spatial channels, N_p is the number of pulses contained in the coherent processing interval, and $\mathbf{n}_l \in \mathbb{C}^{N\times 1}$ is the clutter component. For $\mathbf{s}_i$, we have

$$\mathbf{s}_i = \begin{cases} \alpha\chi_p(-\epsilon_0,\, f)\mathbf{v}, & i = l, \\ \alpha\chi_p(T_p - \epsilon_0,\, f)\mathbf{v}, & i = l+1, \\ 0, & l \neq l, l+1 \end{cases} \tag{2}$$

where α is the complex magnitude of the signal, l is the cell under test, $\chi_p(\cdot,\cdot)$ is the (complex) ambiguity function of the pulse waveform, ε_0 is a residual delay that leads to target energy spillover, f is the target Doppler frequency of the signal backscattered by the target, and $\mathbf{v}$ is the overall space-time steering vector. For the sake of brevity of notations, we omit the dependence on the spatial and the Doppler frequency. In the absence of clutter, using a rectangular pulse of duration T_p s as the radar waveform, the output of the matched filter, i.e., the ambiguity function is triangular (see [23] for further details) as illustrated in Fig. 1.

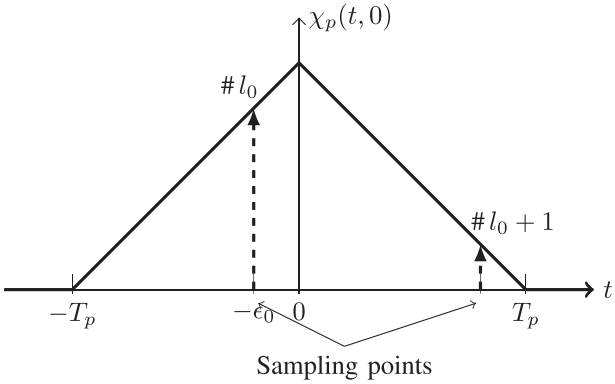

Fig. 1. Illustration of target spillover as sampling of (ambiguity function) output of matched filter for rectangular pulse waveform of duration T_p s.

We further assume that the returns from a coherent pulse train at two different polarimetric channels are sampled simultaneously to the corresponding back-scattered echoes at both polarizations [33–35]. For example, the radar transmits the horizontal polarization (or, equivalently, the vertical polarization) and two linear orthogonal polarizations, denoted as HH and HV (VH and VV), are received. Alternatively, we may assume that both the horizontal and the vertical polarizations are transmitted and that the HH and the VV polarizations are received.

These assumptions imply that the two polarimetric channels receive identical proportion of target spillover with possibly different signal magnitudes as the effective target cross section depends on the polarization. Moreover, the considered polarimetric scenario implies that the N spatial channels use the same polarization modes, for instance, HH and HV, or HH and VV.

In order to facilitate the mathematical derivation and make full use of polarization diversity, we stack the two N-dimensional vectors of the returns, samples from the baseband equivalent at each polarization, and form a $2N$-dimensional vector. Moreover, we alternatively define the residual delay ε evaluated with respect to the ith range subbin accounting for the target position surrounding the lth subbin center as follows

$$\epsilon = \begin{cases} \epsilon_0, & \text{if } i = l \text{ and } 0 \le \epsilon_0 \le T_p/2, \\ \epsilon_0 - T_p, & \text{if } i = l+1 \text{ and } T_p/2 \le \epsilon_0 \le T_p. \end{cases} \tag{3}$$

As customary, we assume that a secondary data $\mathbf{Y} = [\mathbf{y}_1, \ldots, \mathbf{y}_K] \in \mathbb{C}^{2N\times K}$ is available, which does not contain any target echoes and $\mathbf{y}_k$ shares the same covariance matrix as the primary data $\mathbf{X} = [\mathbf{x}_{l-1}, \mathbf{x}_l, \mathbf{x}_{l+1}]$ under the clutter-only hypothesis.

With the above definitions in mind, the decision problem to be solved can be formulated in terms of the following binary hypothesis test:

$$H_0:\begin{cases}\mathbf{x}_{l-1}=\mathbf{n}_1,\ \mathbf{x}_l=\mathbf{n}_2,\ \mathbf{x}_{l+1}=\mathbf{n}_3,\\ \mathbf{y}_k=\mathbf{n}_{k+3}, & k=1,\ldots,K,\end{cases}$$

$$H_1:\begin{cases}\begin{cases}\mathbf{x}_{l-1}=\mathbf{n}_1,\\ \mathbf{x}_{l+1}=\chi_p\left(T_p-\epsilon,\,f\right)\mathbf{V}\boldsymbol{\alpha}+\mathbf{n}_3,\end{cases} & 0<\epsilon\le\frac{T_p}{2},\\ \begin{cases}\mathbf{x}_{l-1}=\chi_p\left(-T_p-\epsilon,\,f\right)\mathbf{V}\boldsymbol{\alpha}+\mathbf{n}_1,\\ \mathbf{x}_{l+1}=\mathbf{n}_3,\end{cases} & -\frac{T_p}{2}\le\epsilon\le 0,\\ \mathbf{x}_l=\chi_p\left(-\epsilon,\,f\right)\mathbf{V}\boldsymbol{\alpha}+\mathbf{n}_2,\\ \mathbf{y}_k=\mathbf{n}_{k+3}, & k=1,\ldots,K,\end{cases} \tag{4}$$

where H_0 and H_1 denote the clutter-only hypothesis and the signal-plus-clutter hypothesis, respectively, $\boldsymbol{\alpha}=[\alpha_1,\alpha_2]^T\in\mathbb{C}^{2\times 1}$ (^{T} denotes transpose) is a complex vector whose elements are parameters accounting for both the channel effects and the target polarimetric characteristics, and $\mathbf{n}_k$, $k=1,\ldots,K+3$, are independent complex normal random vectors with zero mean and covariance matrix $\mathbf{M}$. As to $\mathbf{V}\in\mathbb{C}^{2N\times 2}$, it is given by

$$\mathbf{V}=\begin{pmatrix}\mathbf{v} & \mathbf{0}_{N,1}\\ \mathbf{0}_{N,1} & \mathbf{v}\end{pmatrix} \tag{5}$$

with $\mathbf{v}\in\mathbb{C}^{N\times 1}$ the nominal steering vector, and $\mathbf{0}_{m,n}$ the matrix of $m\times n$ zeros.

III. DETECTOR DESIGN

For the problem in (4), the UMP detector does not exist because the likelihood ratio depends on the unknown covariance matrix. Thus, we aim to find decision statistics that achieve higher detection probability with reasonable computational complexity and result in a CFAR [45]. In order to meet these goals in this section, we derive two suboptimum decision rules using the GLRT and the Wald test, respectively. The GLRT might provide better detection performance than the Wald test, whereas the Wald test might require less computational complexity. Note also that the GLRT and the Wald test can be designed under a CFAR constraint; they are separating function estimation tests and have identical asymptotic performance for large sample sizes (see [46] for more details).

We assume that T_p, $\mathbf{v}$, and f are known a priori, while ε, $\boldsymbol{\alpha}$, and $\mathbf{M}$ need to be estimated. Moreover, we denote by $\mathbf{Z}=[\mathbf{X}\ \mathbf{Y}]\in\mathbb{C}^{2N\times(K+3)}$ the overall data matrix, with $\mathbf{X}=[\mathbf{x}_{l-1},\mathbf{x}_l,\mathbf{x}_{l+1}]\in\mathbb{C}^{2N\times 3}$ the primary data matrix, $\mathbf{Y}=[\mathbf{y}_1,\ldots,\mathbf{y}_K]\in\mathbb{C}^{2N\times K}$ the secondary data matrix, and

$$\boldsymbol{\chi}(\epsilon)=\begin{cases}\left[\chi_p(-T_p-\epsilon,\,f),\,\chi_p(-\epsilon,\,f),\,0\right]^T, & -T_p/2\le\epsilon\le 0,\\ \left[0,\,\chi_p(-\epsilon,\,f),\,\chi_p(T_p-\epsilon,\,f)\right]^T, & 0<\epsilon\le T_p/2.\end{cases} \tag{6}$$

A. The GLRT-Based Detector

The GLRT based on primary and secondary data is given by [47]

$$\frac{\max\limits_{\epsilon,\boldsymbol{\alpha},\mathbf{M}} f_1(\mathbf{Z};\mathbf{M},\boldsymbol{\alpha},\epsilon)}{\max\limits_{\mathbf{M}} f_0(\mathbf{Z};\mathbf{M})}\underset{H_0}{\overset{H_1}{\gtrless}}\eta, \tag{7}$$

where η is the threshold value to be set according to the desired probability of false alarm (P_{fa}), and $f_j(\mathbf{Z};\cdot)$ is the probability density function (PDF) of $\mathbf{Z}$ under H_j, $j=0,1$, i.e., [48]

$$\begin{aligned}f_1(\mathbf{Z};\mathbf{M},\boldsymbol{\alpha},\epsilon)&=\frac{\exp\left\{-\text{tr}\left[\mathbf{M}^{-1}\mathbf{T}_1\right]\right\}}{\left[\pi^{2N}\det(\mathbf{M})\right]^{K+3}}\\ f_0(\mathbf{Z};\mathbf{M})&=\frac{\exp\left\{-\text{tr}\left[\mathbf{M}^{-1}\mathbf{T}_0\right]\right\}}{\left[\pi^{2N}\det(\mathbf{M})\right]^{K+3}}\end{aligned} \tag{8}$$

where $(\cdot)^H$ denotes conjugate transpose, det$(\cdot)$ and tr $(\cdot)$ denote the determinant and the trace of a square matrix, respectively, and

$$\begin{aligned}\mathbf{T}_1&=\left[\mathbf{X}-\mathbf{V}\boldsymbol{\alpha}\boldsymbol{\chi}^T(\epsilon)\right]\left[\mathbf{X}-\mathbf{V}\boldsymbol{\alpha}\boldsymbol{\chi}^T(\epsilon)\right]^H+\mathbf{S},\\ \mathbf{T}_0&=\mathbf{X}\mathbf{X}^H+\mathbf{S}\end{aligned} \tag{9}$$

with $\mathbf{S}=\mathbf{Y}\mathbf{Y}^H$ the K times sample covariance matrix of the secondary data.

In order to compute $\max\limits_{\epsilon,\boldsymbol{\alpha},\mathbf{M}} f_1(\mathbf{Z};\mathbf{M},\alpha,\epsilon)$, observe that the maximum of $f_1(\mathbf{Z};\mathbf{M},\boldsymbol{\alpha},\varepsilon)$ with respect to $\mathbf{M}$ is attained by substituting the true covariance matrix with the sample covariance [1]

$$\widehat{\mathbf{M}}=\frac{1}{K+3}\mathbf{T}_1. \tag{10}$$

Substitution of $\widehat{\mathbf{M}}$ into (8) yields

$$f_1(\mathbf{Z};\widehat{\mathbf{M}},\boldsymbol{\alpha},\epsilon)\propto\det(\mathbf{T}_1)^{-(K+3)}, \tag{11}$$

where $\propto$ stands for proportionality. Maximizing (11) over $\boldsymbol{\alpha}$ is tantamount to the following minimization

$$\min_{\boldsymbol{\alpha}}\ \det\left(\left[\mathbf{X}-\mathbf{V}\boldsymbol{\alpha}\boldsymbol{\chi}^T(\epsilon)\right]\left[\mathbf{X}-\mathbf{V}\boldsymbol{\alpha}\boldsymbol{\chi}^T(\epsilon)\right]^H+\mathbf{S}\right). \tag{12}$$

From (12), a closed-form estimate of $\boldsymbol{\alpha}$ is given by (see Appendix A for the proof)

$$\hat{\boldsymbol{\alpha}}=\frac{\left(\mathbf{V}^H\mathbf{S}_1^{-1}\mathbf{V}\right)^{-1}\mathbf{V}^H\mathbf{S}_1^{-1}\overline{X}}{\|\boldsymbol{\chi}(\epsilon)\|}, \tag{13}$$

where $\|\boldsymbol{\chi}(\epsilon)\|^2=\boldsymbol{\chi}^T(\epsilon)\boldsymbol{\chi}^*(\epsilon)$ and

$$\begin{aligned}&\mathbf{S}_1=\mathbf{S}+\bar{\mathbf{X}}_\perp\bar{\mathbf{X}}_\perp^H,\quad \bar{\mathbf{X}}=\mathbf{X}\bar{\boldsymbol{\chi}}^H,\\ &\bar{\mathbf{X}}_\perp=\mathbf{X}\bar{\boldsymbol{\chi}}_\perp^H,\quad \bar{\boldsymbol{\chi}}=\frac{\boldsymbol{\chi}^T(\epsilon)}{\|\boldsymbol{\chi}(\epsilon)\|}.\end{aligned} \tag{14}$$

In (14), $\bar{\boldsymbol{\chi}}_\perp\in\mathbb{C}^{2\times 3}$ is a matrix orthogonal to $\bar{\boldsymbol{\chi}}$ that satisfies $\bar{\boldsymbol{\chi}}_\perp\bar{\boldsymbol{\chi}}^H=\mathbf{0}_{2,1}$ and $\bar{\boldsymbol{\chi}}_\perp\bar{\boldsymbol{\chi}}_\perp^H=\mathbf{I}_2$, with $\mathbf{I}_n$ the n-dimensional identity matrix. It follows that the

compressed likelihood under H_1 can be written as

$$f_1(\mathbf{Z};\widehat{\mathbf{M}},\hat{\boldsymbol{\alpha}},\epsilon)\propto \det\Big[\big(\mathbf{X}-\mathbf{V}\hat{\boldsymbol{\alpha}}\boldsymbol{\chi}^T(\epsilon)\big)\big(\mathbf{X}-\mathbf{V}\hat{\boldsymbol{\alpha}}\boldsymbol{\chi}^T(\epsilon)\big)^H+\mathbf{S}\Big]^{-(K+3)}. \tag{15}$$

Moreover, the compressed likelihood under H_0 is given by

$$f_0(\mathbf{Z};\widehat{\mathbf{M}})\propto \det\big[\mathbf{X}\mathbf{X}^H+\mathbf{S}\big]^{-(K+3)}. \tag{16}$$

Thus, we conclude that the GLRT for (4) can be recast as

$$\max_{\epsilon\in[-\frac{T_p}{2},\frac{T_p}{2}]}\frac{\det\big[\mathbf{X}\mathbf{X}^H+\mathbf{S}\big]}{\det[(\mathbf{X}-\mathbf{V}\hat{\boldsymbol{\alpha}}\boldsymbol{\chi}^T(\epsilon))(\mathbf{X}-\mathbf{V}\hat{\boldsymbol{\alpha}}\boldsymbol{\chi}^T(\epsilon))^H+\mathbf{S}]}\underset{H_1}{\overset{H_0}{\gtrless}}\eta, \tag{17}$$

where η is the suitable modification of the threshold in (7). To gain additional insight into the test statistic, it is shown in Appendix B that the test statistic can be equivalently expressed as

$$\max_{\epsilon\in[-T_p/2,T_p/2]}\frac{\bar{\mathbf{X}}^H\mathbf{S}_1^{-1}\mathbf{V}\big(\mathbf{V}^H\mathbf{S}_1^{-1}\mathbf{V}\big)^{-1}\mathbf{V}^H\mathbf{S}_1^{-1}\bar{\mathbf{X}}}{1+\bar{\mathbf{X}}^H\mathbf{S}_1^{-1}\bar{\mathbf{X}}}\underset{H_1}{\overset{H_0}{\gtrless}}\eta. \tag{18}$$

For the maximization with respect to ε, we use a grid search because a closed-form estimate of ε (termed as $\hat{\epsilon}$) is not available. More precisely, ε takes on values in $\{\frac{n-N_\epsilon}{2N_\epsilon}T_p\}_{n=0}^{2N_\epsilon}$ with $2\mathrm{N}_\varepsilon$ is the number of search points. In the sequel, we refer to this grid-search implementation as the polarimetric GLRT with localization capabilities (P-GLRT-LC).

B. The Wald Test Detector

In this subsection, we derive a detector based on the Wald test. More precisely, we derive the Wald test assuming that ε is known, then maximize the derived test with respect to ε.

As a preliminary step toward the derivation of the receiver, denote by $\boldsymbol{\theta}\in\mathbb{R}^{4+N^2}$ the parameter vector, i.e.,

$$\boldsymbol{\theta}=[\alpha_{r,1},\alpha_{r,2},\alpha_{i,1},\alpha_{i,2},\mathbf{f}(\mathbf{M})^T]^T=[\boldsymbol{\theta}_A^T\ \boldsymbol{\theta}_B^T]^T, \tag{19}$$

where

1) $\alpha_{r,t}$ and $\alpha_{i,t}$ denote the real and imaginary part of α_t, $t=1,2$;

2) $\boldsymbol{\theta}_A=[\alpha_{r,1},\alpha_{r,2},\alpha_{i,1},\alpha_{i,2}]^T\in\mathbb{R}^4$ and $\boldsymbol{\theta}_B=\mathbf{f}(\mathbf{M})\in\mathbb{R}^{N^2}$; observe that $\boldsymbol{\theta}_A$ contains the parameters of interest while $\boldsymbol{\theta}_B$ contains the nuisance parameters; and

3) $\mathbf{f}(\mathbf{M})\in\mathbb{R}^{N^2}$ is a vector that contains in univocal way the real and the imaginary parts of the elements of $\mathbf{M}$.

Finally, let $\mathbf{J}(\boldsymbol{\theta})$ be the Fisher information matrix, which can be written as follows [49]

$$\mathbf{J}(\boldsymbol{\theta})^{-1}=\begin{bmatrix}\mathbf{J}_{AA}(\boldsymbol{\theta}) & \mathbf{J}_{AB}(\boldsymbol{\theta})\\ \mathbf{J}_{BA}(\boldsymbol{\theta}) & \mathbf{J}_{BB}(\boldsymbol{\theta})\end{bmatrix}^{-1}=\begin{bmatrix}\mathbf{C}_{AA}(\boldsymbol{\theta}) & \mathbf{C}_{AB}(\boldsymbol{\theta})\\ \mathbf{C}_{BA}(\boldsymbol{\theta}) & \mathbf{C}_{BB}(\boldsymbol{\theta})\end{bmatrix}, \tag{20}$$

where

$$\mathbf{C}_{AA}(\boldsymbol{\theta})=\big[\mathbf{J}_{AA}(\boldsymbol{\theta})-\mathbf{J}_{AB}(\boldsymbol{\theta})\mathbf{J}_{BB}^{-1}(\boldsymbol{\theta})\mathbf{J}_{BA}(\boldsymbol{\theta})\big]^{-1}. \tag{21}$$

Step 1. *Known* ε: The Wald test is given by [47]

$$\hat{\boldsymbol{\theta}}_{A,1}^T\Big[\mathbf{C}_{AA}(\hat{\boldsymbol{\theta}}_1)\Big]^{-1}\hat{\boldsymbol{\theta}}_{A,1}\underset{H_1}{\overset{H_0}{\gtrless}}\eta, \tag{22}$$

where $\hat{\boldsymbol{\theta}}_1=[\hat{\boldsymbol{\theta}}_{A,1}^T\ \hat{\boldsymbol{\theta}}_{B,1}^T]^T$ with $\hat{\boldsymbol{\theta}}_{A,1}$ and $\hat{\boldsymbol{\theta}}_{B,1}$ the maximum likelihood estimates of $\boldsymbol{\theta}_A$ and $\boldsymbol{\theta}_B$ under H_1, respectively, and η is the threshold to be set to achieve a predetermined probability of P_{fa}.

For our problem, it is proved in Appendix C that

$$\mathbf{J}_{AA}(\boldsymbol{\theta})=\begin{bmatrix}\mathrm{Re}\{\phi(\boldsymbol{\theta})\} & -\mathrm{Im}\{\phi(\boldsymbol{\theta})\}\\ \mathrm{Im}\{\phi(\boldsymbol{\theta})\} & \mathrm{Re}\{\phi(\boldsymbol{\theta})\}\end{bmatrix},\qquad \mathbf{J}_{AB}(\boldsymbol{\theta})=\mathbf{0}_{4,N^2}, \tag{23}$$

where $\mathrm{Re}\{\cdot\}$ and $\mathrm{Im}\{\cdot\}$ denote the real and the imaginary parts of the argument, respectively, and

$$\phi(\boldsymbol{\theta})=\|\boldsymbol{\chi}(\epsilon)\|^2\mathbf{V}^H\mathbf{M}^{-1}\mathbf{V}. \tag{24}$$

Plugging (23) into (21) yields

$$\mathbf{C}_{AA}(\boldsymbol{\theta})=\begin{bmatrix}\mathrm{Re}\{\phi(\boldsymbol{\theta})\} & -\mathrm{Im}\{\phi(\boldsymbol{\theta})\}\\ \mathrm{Im}\{\phi(\boldsymbol{\theta})\} & \mathrm{Re}\{\phi(\boldsymbol{\theta})\}\end{bmatrix}^{-1}. \tag{25}$$

Moreover, we have

$$\hat{\boldsymbol{\theta}}_{A,1}=\begin{bmatrix}2\mathrm{Re}\{\hat{\boldsymbol{\alpha}}\}\\ 2\mathrm{Im}\{\hat{\boldsymbol{\alpha}}\}\end{bmatrix}=\begin{bmatrix}2\mathrm{Re}\left\{\frac{(\mathbf{V}^H\mathbf{S}_1^{-1}\mathbf{V})^{-1}\mathbf{V}^H\mathbf{S}_1^{-1}\bar{\mathbf{X}}}{\|\boldsymbol{\chi}(\epsilon)\|}\right\}\\ 2\mathrm{Im}\left\{\frac{(\mathbf{V}^H\mathbf{S}_1^{-1}\mathbf{V})^{-1}\mathbf{V}^H\mathbf{S}_1^{-1}\bar{\mathbf{X}}}{\|\boldsymbol{\chi}(\epsilon)\|}\right\}\end{bmatrix}. \tag{26}$$

Now, it remains to replace $\mathbf{M}$ in (24) with its maximum likelihood estimate under H_1, which is given by substituting $\hat{\boldsymbol{\alpha}}$ into (10), i.e.,

$$\widehat{\mathbf{M}}_1=\frac{1}{K+3}\Big(\big[\mathbf{X}-\mathbf{V}\hat{\boldsymbol{\alpha}}\boldsymbol{\chi}^T(\epsilon)\big]\big[\mathbf{X}-\mathbf{V}\hat{\boldsymbol{\alpha}}\boldsymbol{\chi}^T(\epsilon)\big]^H+\mathbf{S}\Big). \tag{27}$$

Observe that

$$\begin{aligned}\mathbf{V}^H\widehat{\mathbf{M}}_1^{-1}\mathbf{V}&=(K+3)\left[\mathbf{V}^H\mathbf{S}_1^{-1}\mathbf{V}-\frac{\mathbf{V}^H\mathbf{S}_1^{-1}\mathbf{p}\mathbf{p}^H\mathbf{S}_1^{-1}\mathbf{V}}{1+\mathbf{p}^H\mathbf{S}_1^{-1}\mathbf{p}}\right]\\&=(K+3)\mathbf{V}^H\mathbf{S}_1^{-1}\mathbf{V},\end{aligned} \tag{28}$$

where $\mathbf{p}=\bar{\mathbf{X}}-\|\boldsymbol{\chi}(\epsilon)\|\mathbf{V}\hat{\boldsymbol{\alpha}}$, and the last equality follows from

$$\mathbf{V}^H\mathbf{S}_1^{-1}\left(\bar{\mathbf{X}}-\|\boldsymbol{\chi}(\epsilon)\|\,\mathbf{V}\hat{\boldsymbol{\alpha}}\right)=\mathbf{0}_{2,1}. \tag{29}$$

It follows that the Wald test can be recast as

$$\bar{\mathbf{X}}^H\mathbf{S}_1^{-1}\mathbf{V}\big(\mathbf{V}^H\mathbf{S}_1^{-1}\mathbf{V}\big)^{-1}\mathbf{V}^H\mathbf{S}_1^{-1}\bar{\mathbf{X}}\underset{H_1}{\overset{H_0}{\gtrless}}\eta. \tag{30}$$

Step 2. *Adaptive Detector*: In order to make the derived detector have the ability to localize a target, we need to maximize (30) with respect to ε, i.e.,

$$\max_{\epsilon\in[-T_p/2,T_p/2]}\bar{\mathbf{X}}^H\mathbf{S}_1^{-1}\mathbf{V}\big(\mathbf{V}^H\mathbf{S}_1^{-1}\mathbf{V}\big)^{-1}\mathbf{V}^H\mathbf{S}_1^{-1}\bar{\mathbf{X}}\underset{H_1}{\overset{H_0}{\gtrless}}\eta. \tag{31}$$

This detector with a grid-search-based implementation will be referred to in the sequel as the polarimetric Wald with localization capabilities (P-WALD-LC).

REMARK 1. The P-GLRT-LC and P-WALD-LC ensure the CFAR property with respect to $\boldsymbol{M}$. Proofs of such statements, not reported here for the sake of brevity, follow the lead of [1] and references therein.

REMARK 2. Comparing the similarity in the expressions [18, 30], we argue and expect that these tests perform very similarly where $\bar{\mathbf{X}}^H\mathbf{S}_1^{-1}\bar{\mathbf{X}}$ is approximately 0, e.g., when the secondary data size that increases their performance gap is expected to reduce.

REMARK 3. Because $\bar{\mathbf{X}}$ and $\mathbf{S}_1^{-1}$ are functions of ε, they need to be calculated for each ε value that involves a heavy computation burden. In order to reduce the computation cost, in Appendix D, we rewrite the expressions in (31) and (18) as

$$\begin{aligned}\beta_{\text{WALD}} &= \left(\mathbf{z}_1 + \frac{\mathbf{z}_1 z_2}{1+z_2}\right)\left(\mathbf{V}^H\mathbf{T}_0^{-1}\mathbf{V} + \frac{\mathbf{z}_1^H\mathbf{z}_1}{1+z_2}\right)^{-1} \\ &\quad\times\left(\mathbf{z}_1 + \frac{\mathbf{z}_1 z_2}{1+z_2}\right)^H \\ \beta_{\text{GLRT}} &= \frac{\beta_{\text{WALD}}}{1+z_2+\frac{z_2^2}{1+z_2}},\end{aligned} \tag{32}$$

where $\mathbf{z}_1 = \mathbf{U}^H\mathbf{V} \in \mathbb{C}^{1\times 2}$, $z_2 = \bar{\mathbf{X}}^H\mathbf{U} \in \mathbb{C}^{1\times 1}$, $\mathbf{U} = \mathbf{T}_0^{-1}\bar{\mathbf{X}} \in \mathbb{C}^{2N\times 1}$, and $\mathbf{T}_0$ given by (9). Thus, we propose the following procedure to calculate the statistics (31) and (18):

S1) Calculate $\mathbf{T}_0^{-1}$ based on the overall data matrix as well as $\mathbf{V}^H\mathbf{T}_0^{-1}\mathbf{V}$. There are $O(8N^3 + 4KN^2 + 8N)$ floating-point operations (flops) involved, where $O(n)$ is the usual Landau notation and means that the implementation requires a number of flops proportional to n [50].

S2) For each ε, calculate $\mathbf{z}_1$ and z_2, and then calculate β_{WALD} as well as β_{GLRT}. The involved computational complexity is $O((4N^2 + 6N) \times (2N_\varepsilon + 1))$.

S3) The maximal values of β_{GLRT} and β_{WALD} are the test statistics of the P-GLRT-LC and P-WALD-LC, respectively.

These proposed procedures involve a computational cost of order of $O(8N^3 + 4KN^2 + 8N + (4N^2 + 6N) \times (2N_\varepsilon + 1))$ flops instead of $O((8N^3 + 4KN^2 + 12N) \times (2N_\varepsilon + 1))$ flops required by directly calculating (31) and (18).

IV. PERFORMANCE ASSESSMENT

This section is devoted to the performance assessment of the proposed detection algorithms in terms of probability of detection (P_{d}) and RMS error in the range. To this end, we compare the proposed detectors with their nonpolarimetric counterparts, i.e., the so-called modified GLRT (M-GLRT) and modified AMF (M-AMF) introduced in [23]. Moreover, the new receivers are compared to the state-of-the-art polarimetric detectors that ignore the spillover, i.e., the polarization-space-time GLRT (P-GLRT) and polarimetric AMF (P-AMF) derived in [29] and [30], respectively.

A. Simulated Data

Because the closed-form expressions for both the P_{fa} and P_{d} are not available, we resort to standard Monte Carlo techniques and evaluate the thresholds necessary to ensure a preassigned value of P_{fa} resorting to $100/P_{\text{fa}}$ independent trials. The P_{d} values and the RMS range errors are estimated over 10^4 and 10^3 independent trials, respectively. All the illustrative examples assume $P_{\text{fa}} = 10^{-4}$, $f_c = 10^9$ Hz, $T_p = 0.2$ μs, $c = 3 \cdot 10^8$ m/s, and $f = 0$ Hz. It is reasonable to assume that the residual position of the target is (independent from trial to trial) uniformly distributed over $(-T_p/2, T_p/2)$. In the sequel, we specify the clutter and target models for the further developments.

Clutter model: We assume a clutter-dominated environment with the covariance matrix given by

$$\mathbf{M} = \mathbf{M}_c \otimes \mathbf{\Sigma}, \tag{33}$$

where $\otimes$ denotes the Kronecker matrix product, $\mathbf{\Sigma} \in \mathbb{C}^{N\times N}$is a matrix that accounts for the covariance between returns from the same polarimetric channel, and

$$\mathbf{M}_c = \begin{pmatrix} 1 & \xi_c\sqrt{\delta_c} \\ \xi_c^*\sqrt{\delta_c} & \delta_c \end{pmatrix} \tag{34}$$

is the clutter polarimetric scattering matrix. As customary, we model $\mathbf{\Sigma}$ as an exponentially shaped matrix with one-lag correlation coefficient ρ_c.

Target model. We consider a fluctuating target, i.e., we use the product model proposed in [41] to describe the aspect angle variability of the target. More precisely, we set $\boldsymbol{\alpha} = \sqrt{\gamma}\mathbf{g}$, where γ is a Gamma random variate with the following PDF

$$f_\gamma(x) = \frac{1}{\bar{\gamma}\Gamma(\nu)}\left(\frac{x}{\bar{\gamma}}\right)^{\nu-1}\exp\left\{-\frac{x}{\bar{\gamma}}\right\}, \tag{35}$$

and $\Gamma(\cdot)$ is the Eulerian gamma function, ν is the shape parameter, and the scale parameter $\bar{\gamma}$ is related to the mean radar cross section. The zero-mean complex Gaussian bivariate $\mathbf{g}$ has the covariance matrix of

$$\mathbf{M}_t = \begin{pmatrix} 1 & \xi_t\sqrt{\delta_t} \\ \xi_t^*\sqrt{\delta_t} & \delta_t \end{pmatrix}. \tag{36}$$

The typical values of ξ_c, δ_c, ξ_t, δ_t are obtained from Table I of [41]. Some of them were not explicitly provided in [37], such as ε_t and ε_c. However, they can be easily computed using Table 1 of [37]. These parameters are for the polarimetric measurement data of typical ground targets and meadow clutter, and have been widely exploited in most existing works, such as [33–35]. According to above assumptions, the signal-to-clutter ratio (SCR) is defined as

$$\begin{aligned}\text{SCR} &= E\left[\boldsymbol{\alpha}^H\left(\mathbf{V}\mathbf{M}^{-1}\mathbf{V}\right)\boldsymbol{\alpha}\right] \\ &= \nu\bar{\gamma}\mathbf{v}^H\mathbf{\Sigma}^{-1}\mathbf{v}\text{tr}\left[\mathbf{M}_t^{1/2}\mathbf{M}_c^{-1}\mathbf{M}_t^{1/2}\right].\end{aligned} \tag{37}$$

TABLE I
Specifications of the Analyzed Sea Clutter Dataset

	Dataset226
Date	November 17, 1993
Time	13.16
Number of pulses N_t	12288
Number of cells N_s	68
Polarizations	HH, VV
RF frequency	9.39 GHz
Pulse length	200 ns
Pulse repetition frequency	1000 Hz
Sampling frequency	10 MHz
Radar scan mode	Fixed azimuth
Radar azimuth angle	135.0439 deg
Elevation angle	359.5111 deg
Range	2001–3006 m
Radar beam width	0.9 deg
Range resolution	30 m sampled at 15 m
Quantization bit	8 bit
Mean/max wind speed	20 km/h
Sea state: mean/max wave height	1/1.6 m

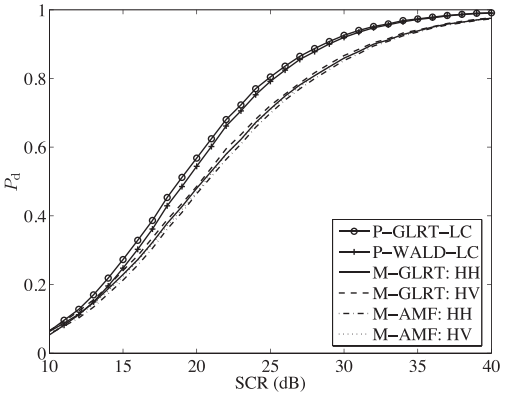

Fig. 2. P_d versus SCR for P-GLRT-LC, P-WALD-LC that process HH and HV channels, and M-GLRT and M-AMF that process single polarimetric channel with simulated data; $N = 8$, $K = 32$, $N_\varepsilon = 5$, $P_{fa} = 10^{-4}$, $v = 1.0$, $\rho_c = 0.9$, $\xi_t = 0$, $\delta_t = 0.19$, $\xi_c = 0$, $\delta_c = 0.18$.

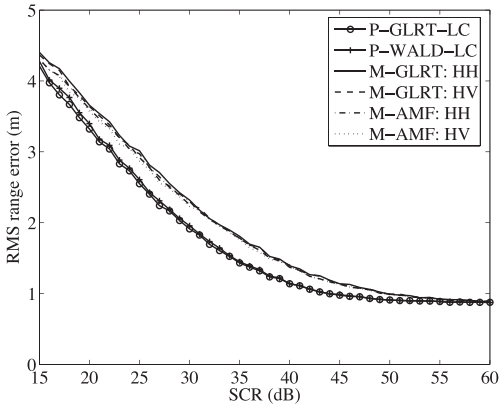

Fig. 3. RMS errors in range versus SCR for P-GLRT-LC, P-WALD-LC that process HH and HV channels, and M-GLRT and M-AMF that process single polarimetric channel with simulated data; $N = 8$, $K = 24$, $N_\varepsilon = 5$, $P_{fa} = 10^{-4}$, $v = 1.0$, $\rho_c = 0.9$, $\xi_t = 0$, $\delta_t = 0.19$, $\xi_c = 0$, $\delta_c = 0.18$.

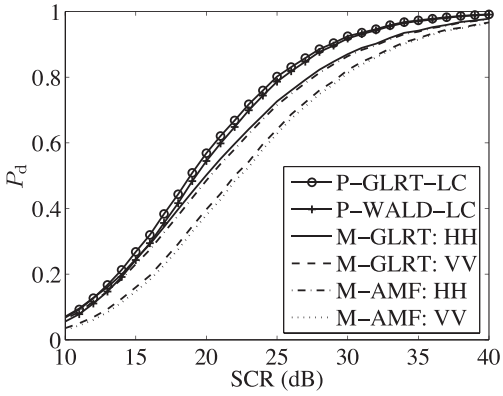

Fig. 4. P_d versus SCR for P-GLRT-LC, P-WALD-LC that process HH and VV channels, and M-GLRT and M-AMF that process single polarimetric channel with simulated data; $N = 8$, $K = 32$, $N_\varepsilon = 5$, $P_{fa} = 10^{-4}$, $v = 1.0$, $\rho_c = 0.9$, $\xi_t = 0.28$, $\delta_t = 1$, $\xi_c = 0.5$, $\delta_c = 1.6$.

It is worth mentioning that when HH and HV (or, equivalently, VV and VH) are employed, target and clutter returns at different channels can be assumed independent random vectors and, hence, $\xi_c = \xi_t = 0$.

1) *Comparison with Localization Detectors*. In Figs. 2 and 3, we compare the P-GLRT-LC and P-WALD-LC with the M-GLRT and M-AMF, assuming $N = 8$, $K = 32$, $v = 1$, $\rho_c = 0.9$, and $N_\varepsilon = 5$. In particular, in Fig. 2 we plot P_d versus SCR, while in Fig. 3 the comparisons are in terms of range RMS error. Moreover, the figures refer to a radar that processes the HH and the HV channels. Accordingly, we set $\xi_t = 0$, $\delta_t = 0.19$, $\xi_c = 0$, $\delta_c = 0.18$ [41]. We used the target 1 mode and have not changed these parameters during the simulations.

The curves in Fig. 2 show that the P-GLRT-LC and P-WALD-LC guarantee better detection performance than the M-GLRT and M-AMF, which only process the HH or HV channel. More precisely, the P-GLRT-LC have the best performance, whereas the P-WALD-LC experiences a loss of about 0.3 dB at $P_d = 0.9$; such a loss increases to about 3.0 dB for the M-GLRT and M-AMF. On the other hand, Fig. 3 shows that the P-GLRT-LC and P-WALD-LC have superior performance in terms of capability of target localization with respect to the M-GLRT and M-AMF. For instance, the range RMS errors of the P-GLRT-LC and P-WALD-LC are about 2.5 m when SCR = 25 dB, and such RMS errors increase to about 2.9 m for the M-GLRT and M-AMF. These results highlight the benefits provided by polarimetric diversity, i.e., the polarization diversity enhances the performance of a radar system about 3 dB in SCR.

The trend observed in Figs. 2 and 3 is confirmed by the curves in Figs. 4 and 5, for the same parameters and employing the HH and VV channels. Following [41], we set $\xi_t = 0.28$, $\delta_t = 1$, $\xi_c = 0.5$, $\delta_c = 1.6$. An interesting phenomenon is that the P_d curves for the M-GLRT and M-AMF using the HH channel are higher than those using the VV channel. As to the range RMS errors, the curves using the HH channel are lower than those using the VV

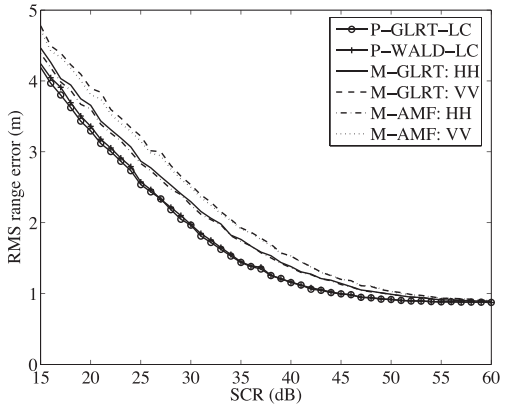

Fig. 5. RMS errors in range versus SCR for P-GLRT-LC, P-WALD-LC that process HH and VV channels, and M-GLRT and M-AMF that process single polarimetric channel with simulated data; $N = 8$, $K = 32$, $N_\varepsilon = 5$, $P_{\text{fa}} = 10^{-4}$, $v = 1.0$, $\rho_c = 0.9$, $\xi_t = 0.28$, $\delta_t = 1$, $\xi_c = 0.5$, $\delta_c = 1.6$.

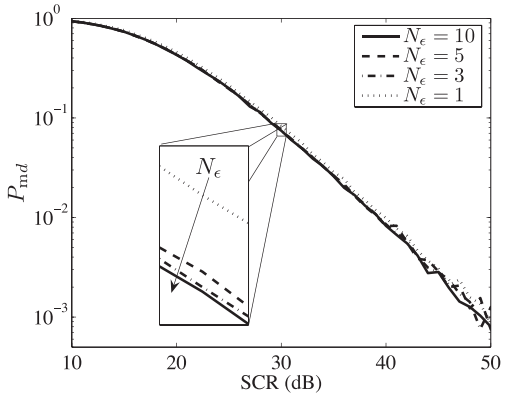

Fig. 6. P_{md} versus SCR for P-GLRT-LC that processes HH and HV channels with simulated data; $N = 8$, $K = 32$, $P_{\text{fa}} = 10^{-4}$, $v = 1.0$, $\rho_c = 0.9$, $\xi_t = 0$, $\delta_t = 0.19$, $\xi_c = 0$, $\delta_c = 0.18$, and several cases of N_ε.

channel. We argue that this performance difference is because of $\frac{\delta_t}{\delta_c} < 1$, which means the HH channel has higher SCR than the VV channel.

In the above simulations, we use a fixed value for N_ε that obviously limits the accuracy of the range estimation. In fact, at very high SCRs using a grid search over ε, the range estimation error is an uniformly distributed random variable over $(-\frac{T_p c}{4N_\epsilon}, \frac{T_p c}{4N_\epsilon})$ and has a standard deviation equal to $\frac{T_p c}{8\sqrt{3}N_\epsilon}$. For example in Fig. 3, we observe a range RMS error of 0.88 m, which is comparable with $\frac{T_p c}{8\sqrt{3}N_\epsilon} = 0.866$ m for $N_\varepsilon = 5$ [23]. In Fig. 6, we study the effect of N_ε on the detection performance of the P-GLRT-LC. Therein, we plot the probability of miss detection (P_{md}) versus SCR for $N_\varepsilon\{1, 3, 10\}$ where other parameters are set the same as in Fig. 2. The figure shows that the improvement of the detection performance is quickly saturated as N_ε increases. Compared with the increased computational complexity for large N_ε, the improvement on the detection probability may be insignificant whereas the improvement on the accuracy of localization is

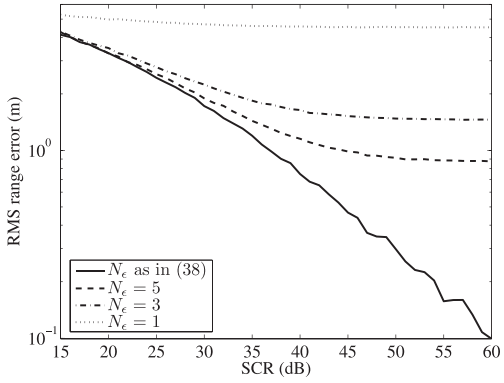

Fig. 7. RMS errors in range versus SCR for P-GLRT-LC that processes HH and HV channels with simulated data; $N = 8$, $K = 32$, $P_{\text{fa}} = 10^{-4}$, $v = 1.0$, $\rho_c = 0.9$, $\xi_t = 0$, $\delta_t = 0.19$, $\xi_c = 0$, $\delta_c = 0.18$, and several cases of N_ε.

considerable. Hence, the main incentive to use larger values for N_ε is to enhance the range accuracy.

For large values of N_ε, the variance of $\hat{\epsilon}$ is proportional to the variance of the clutter, i.e., proportional to $10^{-\frac{\text{SCR}}{10}}$ (SCR in decibels). Moreover, the quantization errors of $\hat{\epsilon}$ is proportional to $\frac{1}{N_\epsilon^2}$. This means that it is reasonable to choose $\frac{1}{N_\epsilon^2}$ to be proportional to $10^{-\frac{SCR}{10}}$. Thus, to have a reasonable trade-off between the performance and computational cost, we propose to choose N_ε as

$$N_\epsilon = \left\lceil c \times 10^{\frac{SCR}{20}} + 2 \right\rceil, \tag{38}$$

where $\lceil \cdot \rceil$ denotes the smallest integer not less than the parameter, and $c = 0.316$ is an empirical value. Fig. 7 shows the effect of (38) on the range estimation, i.e., the range RMS error versus SCR of the P-GLRT-LC for $N_\varepsilon \varepsilon \{1, 3, 5\}$ and for N_ε calculated by (38). Fig. 7 highlights that by using (38), we obtain lower range RMS errors for medium-high SCR values than the fixed values of N_ε. Moreover, the higher the SCR values, the superior the range estimation capability with respect to the fixed values. The above results suggest selecting N_ε based on the system requirements. If only the detection performance is important, we may use some small value for N_ε and use (38) for most accurate range estimation. To save simulation time hereafter, we fix value of N_ε.

2) *Comparison with Polarimetric Detectors*. In Figs. 8 and 9, we compare new receivers with state-of-the-art polarimetric detectors. Specifically, we plot P_{d} versus SCR for the P-GLRT-LC, P-WALD-LC, P-GLRT, and P-AMF, assuming $N = 8$, $N_\varepsilon = 5$, $v = 1$, $\rho_c = 0.9$, and two values of K. Fig. 8 refers to a radar that processes the HH and the HV channels, whereas Fig. 9 corresponds to a system employing the HH and VV channels. The figures show that the P-GLRT-LC and P-WALD-LC outperform the P-GLRT and P-AMF in detection performance. Moreover, the smaller the K, the higher the P_{d} of the P-GLRT-LC with respect to other three detectors. For instance, the P_{d} gain of the P-GLRT-LC with respect to the P-WALD-LC is 1.2 dB for $P_{\text{d}} = 0.9$ and $K = 20$, and such gain reduces

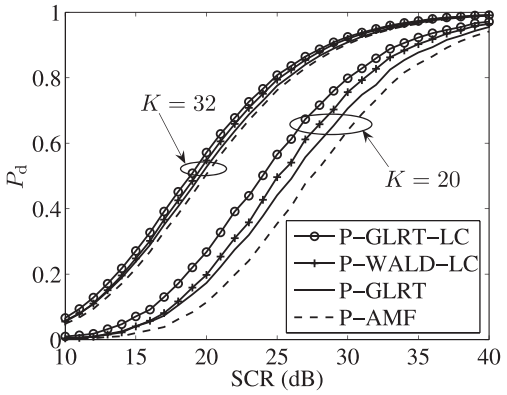

Fig. 8. P_d versus SCR for P-GLRT-LC, P-WALD-LC that process HH and HV channels, and P-GLRT and P-AMF with simulated data; $N = 8$, $N_\varepsilon = 5$, $P_{fa} = 10^{-4}$, $v = 1.0$, $\rho_c = 0.9$, $\xi_t = 0$, $\delta_t = 0.19$, $\xi_c = 0$, $\delta_c = 0.18$, and K as parameter.

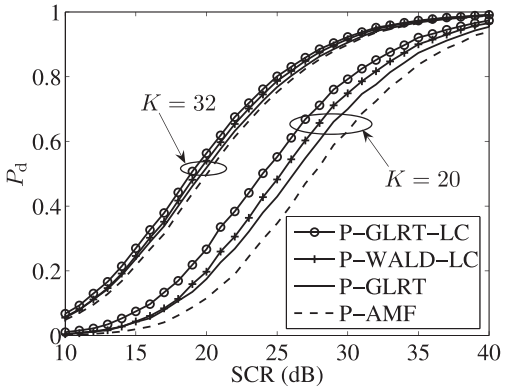

Fig. 9. P_d versus SCR for P-GLRT-LC and P-WALD-LC that process HH and VV channels, and P-GLRT and P-AMF with simulated data; $N = 8$, $N_\varepsilon = 5$, $P_{fa} = 10^{-4}$, $v = 1.0$, $\rho_c = 0.9$, $\xi_t = 0.28$, $\delta_t = 1$, $\xi_c = 0.5$, $\delta_c = 1.6$, and K as parameter.

to about 0.3 dB for $K = 32$. This result is accordance with what we expect in Remark 2. We do not evaluate the range RMS errors for the considered detectors due to the fact that the P-GLRT and P-AMF do not have the ability of subbin range localization. In summary, the performed analysis highlights that the proposed receivers result in enhanced performances compared to the receivers that exploit either polarimetric diversity or the energy spillover of the target.

B. Real Dataset

In the above simulations, the clutter is generated by a complex Gaussian process, which matches the design model. In this subsection, we present a performance analysis based on the real radar measurements collected by the McMaster IPIX radar, which contain many challenging real-world effects, including heterogeneous terrain and array errors. Specifically, the measurements were collected in November 1993 using the McMaster IPIX radar from a site in Dartmouth. The radar was mounted on a cliff facing the Atlantic Ocean, at a height of 100 feet above the mean sea level and was used in fixed azimuth mode. The IPIX radar employed a coherent receiver and was capable of

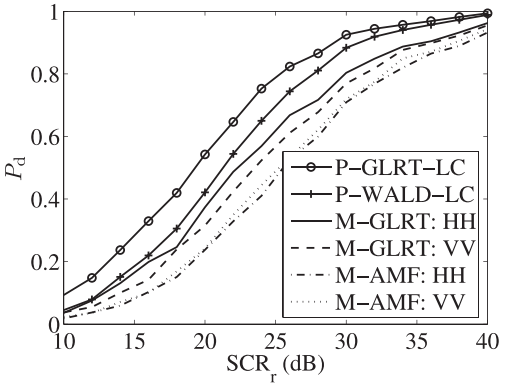

Fig. 10. P_d versus SCR for P-GLRT-LC, P-WALD-LC that process HH and VV channels, and M-GLRT and M-AMF that process single polarimetric channel with IPIX data; $N = 8$, $K = 32$, $N_\varepsilon = 5$, FA = 15, $v = 1.0$, $\xi_t = 0.28$, $\delta_t = 1$.

operating in a dual-polarized mode. More details on the experiment can be found in [51]. The specifications of the considered dataset containing are reported in Table I.

For the analysis, the nominal steering vector is temporal (namely $N = N_p$). We use the data in range cells 49–51 as the primary data, and the range cells adjacent to the primary data as the secondary data. Moreover, there are two guard cells between the primary data and secondary data, namely, the range cells 31–46 and 54–69 for $K = 32$. The resulting $N(K + 3)$ data window, centered on the CUT, is slid in index N along the 12 288 time pulses until the end of the dataset. The total number of different data windows is $\lfloor \frac{12288}{N} \rfloor$, where $\lfloor \cdot \rfloor$ denotes the nearest integer less than or equal to the argument. This number coincides with the total number of trials used to estimate both the number of false alarms (FA) and P_d of each receiver.

We investigate the behaviors of the P-GLRT-LC and P-AMF-LC under the same number of FA because the limited amount of real data do not allow a Monte Carlo estimation of the P_{fa}. Specifically, we set FA = 15, which corresponds to an obtained P_{fa} of about 10^{-2}. As to target parameters, we set $\xi_t = 0.28$ and $\delta_t = 1$. This is because the considered real data are collected from HH and VV channels. In order to evaluate the P_d, we simulate a synthetic target using the same model as in sub-Section IVA and inject it into the 49th–51st cells. We set the Doppler frequency f at 0 Hz, which is tantamount to considering the worst case of target embedded in deep clutter coinciding with the peak of the clutter power spectral density [52].

Figs. 10 and 11 show the P_d and the range RMS errors of different detectors versus SCR_r, respectively, for $N = 8$, $K = 32$, and $N_\varepsilon = 5$. The SCR_r is defined as

$$SCR_r = E\left[\boldsymbol{\alpha}^H \left(\mathbf{V}\tilde{\mathbf{M}}^{-1}\mathbf{V}\right)\boldsymbol{\alpha}\right] \tag{39}$$

where $\tilde{\mathbf{M}}$ is the estimated sample covariance matrix using all the returns of the range cells 49-51.

Inspection of Figs. 10 and 11 highlights that P-GLRT-LC and P-WALD-LC ensure better performances in terms of both detection and range estimation than the

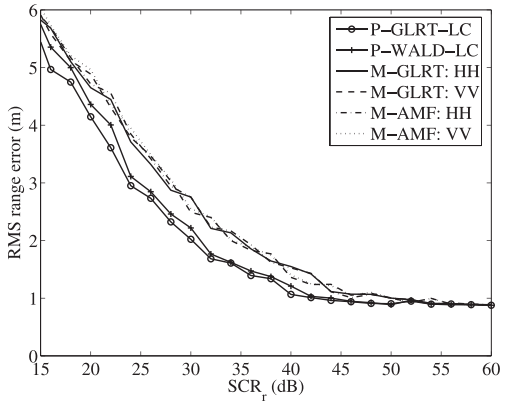

Fig. 11. RMS errors in range versus SCR for P-GLRT-LC, P-WALD-LC that process HH and VV channels, and M-GLRT and M-AMF that process single polarimetric channel with IPIX data; $N = 8$, $K = 32$, $N_\varepsilon = 5$, FA $= 15$, $\upsilon = 1.0$, $\xi_t = 0.28$, $\delta_t = 1$.

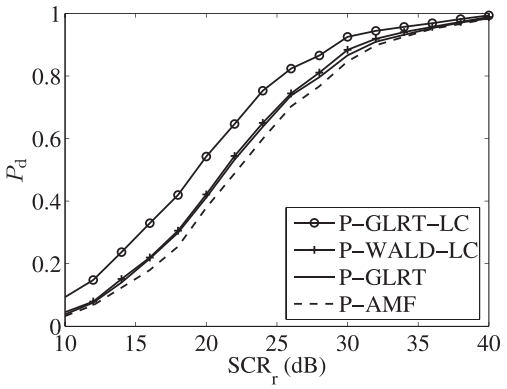

Fig. 12. $P_{\rm d}$ versus SCR for P-GLRT-LC and P-WALD-LC that process HH and VV channels, and P-GLRT and P-AMF with IPIX data; $N = 8$, $K = 32$, $N_\varepsilon = 5$, FA $= 15$, $\upsilon = 1.0$, $\rho_c = 0.9$, $\xi_t = 0.28$, $\delta_t = 1$.

M-GLRT and M-AMF, which agrees with that observed on simulated data. Meanwhile, for low-medium SCR values, the P-GLRT-LC has a little lower range RMS error than the P-WALD-LC. As for high SCR values, the RMS errors become identical due to the fact that they achieve the lower bound given by the grid resolution. On the other hand, Fig. 12 shows that the proposed detectors enhance the detection performance compared with the state-of-the-art polarimetric detectors [29, 30] by exploiting the spillover of target energy. It is also seen that the P-GLRT performs very close to the P-WALD-LC and experiences a loss of about 0.4 dB at $P_{\rm d} = 0.9$. As in [53–55], we conjuncture that the existing gap between the curves for the experimental data and the simulated ones should be caused by the covariance mismatch in the range cells of the experimental dataset.

As a final remark, the case where the M-GLRT and M-AMF process both polarimetric channels is equivalent to doubling the number of antennas for these two detectors; they still exhibit a performance loss with respect to the P-GLRT-LC and P-WALD-LC. This is because they are not operating under the assumed conditions for which they are designed, namely, $\alpha_1 \neq \alpha_2$.

V. CONCLUSIONS

In the present work, we have proposed two adaptive decision schemes with enhanced detection and range estimation capabilities for point-like targets buried in Gaussian clutter with unknown covariance matrix. For the sake of deriving these new detectors, we jointly exploited the polarization diversity information as well as the spillover of target energy to consecutive range samples and used the plain GLRT and the Wald test. Remarkably, both of them possessed the CFAR property with respect to the unknown clutter covariance matrix. The performance assessment, carried out using simulated data and the IPIX dataset, confirmed that the proposed polarimetric detectors outperformed their nonpolarimetric counterparts in terms of probability of detection and range estimation. Moreover, they could provide superior detection performance with respect to the state-of-the-art polarimetric detectors that do not consider the spillover. Future work will involve the extension of our results to the case of more than two channels [31, 32] in order to further improve the detection and range estimation performances. It is also of interest to extend the proposed framework to detect multiple point-like targets [56] or operate under non-Gaussian clutter [57–59].

ACKNOWLEDGMENT

We thank the Associate Editor Ram Narayanan and three anonymous referees who provided insightful comments and constructive criticisms that greatly improved the manuscript.

APPENDIX A. DERIVATION OF THE CLOSED-FORM ESTIMATE OF α

In this appendix, we give the proof of (13). From the definitions in (14), it is easy to prove that

$$\bar{\boldsymbol{\chi}}^H \bar{\boldsymbol{\chi}} + \bar{\boldsymbol{\chi}}_\perp^H \bar{\boldsymbol{\chi}}_\perp = \mathbf{I}_3. \tag{40}$$

Multiplying $\mathbf{X}$ by $\mathbf{I}_3$ on the right and using (40), we have

$$\begin{aligned} \mathbf{X} &= \bar{\mathbf{X}}\bar{\boldsymbol{\chi}} + \bar{\mathbf{X}}_\perp \bar{\boldsymbol{\chi}}_\perp, \\ \mathbf{X}\mathbf{X}^H &= \bar{\mathbf{X}}\bar{\mathbf{X}}^H + \bar{\mathbf{X}}_\perp \bar{\mathbf{X}}_\perp^H. \end{aligned} \tag{41}$$

This easily yields

$$\mathbf{T}_1 = \left(\bar{\mathbf{X}} - \|\boldsymbol{\chi}(\epsilon)\|\,\mathbf{V}\boldsymbol{\alpha}\right)\left(\bar{\mathbf{X}} - \|\boldsymbol{\chi}(\epsilon)\|\,\mathbf{V}\boldsymbol{\alpha}\right)^H + \mathbf{S}_1, \tag{42}$$

where $\mathbf{S}_1$ is given by (14).

The optimization problem in (12) can be expressed as

$$\begin{aligned} &\min_{\boldsymbol{\alpha}} \det\left[\left(\bar{\mathbf{X}} - \|\boldsymbol{\chi}(\epsilon)\|\,\mathbf{V}\boldsymbol{\alpha}\right)\left(\bar{\mathbf{X}} - \|\boldsymbol{\chi}(\epsilon)\|\,\mathbf{V}\boldsymbol{\alpha}\right)^H + \mathbf{S}_1\right] \\ &= \det[\mathbf{S}_1]\left[1 + \left(\bar{\mathbf{X}} - \|\boldsymbol{\chi}(\epsilon)\|\,\mathbf{V}\boldsymbol{\alpha}\right)^H \mathbf{S}_1^{-1}\left(\bar{\mathbf{X}} - \|\boldsymbol{\chi}(\epsilon)\|\,\mathbf{V}\boldsymbol{\alpha}\right)\right], \end{aligned} \tag{43}$$

The derivative of the last factor in (43) with respect to $\boldsymbol{\alpha}$ is given by

$$\frac{\partial}{\partial \boldsymbol{\alpha}}\left[1 + \left(\bar{\mathbf{X}} - \|\boldsymbol{\chi}(\epsilon)\|\,\mathbf{V}\boldsymbol{\alpha}\right)^H \mathbf{S}_1^{-1}\left(\bar{\mathbf{X}} - \|\boldsymbol{\chi}(\epsilon)\|\,\mathbf{V}\boldsymbol{\alpha}\right)\right]$$

$$= \|\boldsymbol{\chi}(\epsilon)\| \mathbf{V}^H \mathbf{S}_1^{-1} \left(\bar{\mathbf{X}} - \|\boldsymbol{\chi}(\epsilon)\| \mathbf{V}\boldsymbol{\alpha}\right). \quad (44)$$

Because $\mathbf{V}$ has full column rank 2, $\mathbf{V}^H\mathbf{S}_1^{-1}\mathbf{V}$ is positive definite and invertible. Setting (44) to zero yields (13).

APPENDIX B. DERIVATION OF (18)

By using (13) and Appendix A, we have

$$f_1(\mathbf{Z}; \widehat{\mathbf{M}}, \hat{\alpha}, \epsilon) \propto \det[\mathbf{S}_1]\left[1 + \bar{\mathbf{X}}^H \mathbf{Q} \bar{\mathbf{X}}\right] \quad (45)$$

where

$$\mathbf{Q} = \mathbf{S}_1^{-1} - \mathbf{S}_1^{-1}\mathbf{V}\left(\mathbf{V}^H\mathbf{S}_1^{-1}\mathbf{V}\right)^{-1}\mathbf{V}^H\mathbf{S}_1^{-1}. \quad (46)$$

It follows that (17) can be recast as

$$\frac{\det\left[\mathbf{X}\mathbf{X}^H + \mathbf{S}\right]}{\det[\mathbf{S}_1]\left[1 + \bar{\mathbf{X}}^H\mathbf{Q}\overline{\mathbf{X}}\right]} = \frac{1 + \bar{\mathbf{X}}^H\mathbf{S}_1^{-1}\bar{\mathbf{X}}}{1 + \bar{\mathbf{X}}^H\mathbf{S}_1^{-1}\bar{\mathbf{X}} - \bar{\mathbf{X}}^H\mathbf{S}_1^{-1}\mathbf{V}\left(\mathbf{V}^H\mathbf{S}_1^{-1}\mathbf{V}\right)^{-1}\mathbf{V}^H\mathbf{S}_1^{-1}\bar{\mathbf{X}}}. \quad (47)$$

It is easy to show that (47) is equivalent to (18).

APPENDIX C. DERIVATION OF THE FISHER INFORMATION MATRIX

Let us begin with $\mathbf{J}_{AA}(\boldsymbol{\theta})$, which is the 4×4 matrix whose (i, j)th entry is

$$\mathbf{J}_{AA}(\boldsymbol{\theta})(i, j) = -E\left[\frac{\partial \ln f_1(\mathbf{Z}; \mathbf{M}, \boldsymbol{\theta})}{\partial \boldsymbol{\theta}_A(i)\boldsymbol{\theta}_A(j)}\right],\ i, j \in (1, 2) \quad (48)$$

where $\boldsymbol{\theta}_A(t)$ denotes the tth element of the vector $\boldsymbol{\theta}_A$.

It can be shown that for $\forall l, k \text{in}(1, 2)$,

$$\begin{aligned}
&\frac{\partial \ln f_1(\mathbf{Z}; \mathbf{M}, \boldsymbol{\theta})}{\partial\alpha_{r,l}\partial\alpha_{r,k}} \\
&\quad = -2\text{Re}\left\{\text{tr}\left[\boldsymbol{\chi}^*(\epsilon)\mathbf{e}_l^T\mathbf{V}^H\mathbf{M}^{-1}\mathbf{V}\mathbf{e}_k\boldsymbol{\chi}^T(\epsilon)\right]\right\} \\
&\frac{\partial \ln f_1(\mathbf{Z}; \mathbf{M}, \boldsymbol{\theta})}{\partial\alpha_{r,l}\partial\alpha_{i,k}} \\
&\quad = \begin{cases} 2\text{Im}\left\{\text{tr}\left[\boldsymbol{\chi}^*(\epsilon)\mathbf{e}_l^T\mathbf{V}^H\mathbf{M}^{-1}\mathbf{V}\mathbf{e}_k\boldsymbol{\chi}^T(\epsilon)\right]\right\}, & l \neq k \\ 0, & l = k \end{cases} \\
&\frac{\partial \ln f_1(\mathbf{Z}; \mathbf{M}, \boldsymbol{\theta})}{\partial\alpha_{i,l}\partial\alpha_{i,k}} \\
&\quad = -2\text{Re}\left\{\text{tr}\left[\boldsymbol{\chi}^*(\epsilon)\boldsymbol{e}_l^T\mathbf{V}^H\mathbf{M}^{-1}\mathbf{V}\mathbf{e}_k\boldsymbol{\chi}^T(\epsilon)\right]\right\} \\
&\frac{\partial \ln f_1(\mathbf{Z}; \mathbf{M}, \boldsymbol{\theta})}{\partial\alpha_{i,l}\partial\alpha_{r,k}} \\
&= \begin{cases} 2\text{Im}\left\{\text{tr}\left[\boldsymbol{\chi}^*(\epsilon)\mathbf{e}_l^T\mathbf{V}^H\mathbf{M}^{-1}\mathbf{V}\mathbf{e}_k\boldsymbol{\chi}^T(\epsilon)\right]\right\}, & l \neq k \\ 0, & l = k, \end{cases}
\end{aligned} \quad (49)$$

where $\mathbf{e}_1 = [1, 0]^T$, and $\mathbf{e}_2 = [0, 1]^T$.

It follows that $\mathbf{J}_{AA}(\boldsymbol{\theta})$ can be recast as

$$\mathbf{J}_{AA}(\boldsymbol{\theta}) = \begin{bmatrix} \text{Re}\{\phi(\boldsymbol{\theta})\} & -\text{Im}\{\phi(\boldsymbol{\theta})\} \\ \text{Im}\{\phi(\boldsymbol{\theta})\} & \text{Re}\{\phi(\boldsymbol{\theta})\} \end{bmatrix}, \quad (50)$$

where $\phi(\boldsymbol{\theta})$ is given by (24). On the other hand, $\mathbf{J}_{AB}(\boldsymbol{\theta})$ is a $4 \times N^2$ matrix whose (i, j)th element is

$$\mathbf{J}_{AB}(\boldsymbol{\theta})(i, j) = -E\left[\frac{\partial \ln f_1(\mathbf{Z}; \mathbf{M}, \boldsymbol{\theta})}{\partial\boldsymbol{\theta}_A(i)\boldsymbol{\theta}_B(j)}\right], \quad i \in (1, \ldots, 4),\ j \in (1, \ldots N^2) \quad (51)$$

where $\boldsymbol{\theta}_B(t)$ denotes the tth element of the vector $\boldsymbol{\theta}_B$. It is easy to show that $\mathbf{J}_{AB}(\boldsymbol{\theta})(i, j)$ are linear function of $[\mathbf{X} - \mathbf{V}\boldsymbol{\alpha}\boldsymbol{\chi}^T(\varepsilon)]$. Thus, we can conclude that $\mathbf{J}_{AB}(\boldsymbol{\theta}) = \mathbf{0}_{4,N^2}$, because of $E[\mathbf{X} - \mathbf{V}\boldsymbol{\alpha}\boldsymbol{\chi}^T(\varepsilon)] = \mathbf{0}_{2N,3}$.

APPENDIX D. DERIVATION OF (32)

Observe that $\mathbf{S}_1$ can be written as

$$\mathbf{S}_1 = \mathbf{T}_0 - \bar{\mathbf{X}}\bar{\mathbf{X}}^H. \quad (52)$$

Using the generalized Woodbury identity [60], we have

$$\mathbf{S}_1^{-1} = \mathbf{T}_0^{-1} + \frac{\mathbf{T}_0^{-1}\bar{\mathbf{X}}\bar{\mathbf{X}}^H\mathbf{T}_0^{-1}}{1 + \bar{\mathbf{X}}^H\mathbf{T}_0^{-1}\bar{\mathbf{X}}}. \quad (53)$$

It follows that

$$\begin{aligned}
\bar{\mathbf{X}}^H\mathbf{S}_1^{-1}\bar{\mathbf{X}} &= \bar{\mathbf{X}}^H\mathbf{T}_0^{-1}\bar{\mathbf{X}} + \frac{\left(\bar{\mathbf{X}}^H\mathbf{T}_0^{-1}\bar{\mathbf{X}}\right)^2}{1 + \bar{\mathbf{X}}^H\mathbf{T}_0^{-1}\bar{\mathbf{X}}} \\
&= z_2 + \frac{z_2^2}{1 + z_2}.
\end{aligned} \quad (54)$$

Similarly, $\bar{\mathbf{X}}^H\mathbf{S}_1^{-1}\mathbf{V}$and $\mathbf{V}^H\mathbf{S}_1^{-1}\mathbf{V}$ can be recast as

$$\bar{\mathbf{X}}^H\mathbf{S}_1^{-1}\mathbf{V} = \mathbf{z}_1 + \frac{\mathbf{z}_1 z_2}{1 + z_2}, \quad (55)$$

$$\mathbf{V}^H\mathbf{S}_1^{-1}\mathbf{V} = \mathbf{V}^H\mathbf{T}_0^{-1}\mathbf{V} + \frac{\mathbf{z}_1^H\mathbf{z}_1}{1 + z_2}. \quad (56)$$

Plugging (54)–(56) into (31) and (18), we obtain (32).

REFERENCES

[1] Kelly, E. J.
An adaptive detection algorithm.
IEEE Transactions on Aerospace and Electronic Systems, **22**, 2 (Mar. 1986), 115–127.

[2] Robey, F. C., Fuhrman, D. L., Kelly, E. J., and Nitzberg R.
A CFAR adaptive matched filter detector.
IEEE Transactions on Aerospace and Electronic Systems, **29**, 1 (Jan. 1992), 208–216.

[3] Conte, E., De Maio, A., and Ricci, G.
GLRT-based adaptive detection algorithms for range-spread targets.
IEEE Transactions on Signal Processing, **49**, 7 (Jul. 2001), 1336–1348.

[4] Bruyere, D. P., and Goodman, N. A.
Adaptive detection and diversity order in multistatic radar.
IEEE Transactions on Aerospace and Electronic Systems, **44**, 4 (Oct. 2008), 1615–1623.

[5] Abramovich, Y. I., Spencer, N. K., and Gorokhov, A. Y.
A modified GLRT and AMF framework for adaptive detectors.
IEEE Transactions on Aerospace and Electronic Systems, **43**, 3 (Jul. 2007), 1017–1051.

[6] De Maio, A., Farina, A., and Foglia, G.
Knowledge-aided Bayesian radar detectors & their application to live data.

IEEE Transactions on Aerospace and Electronic Systems, **46**, 1 (Jan. 2010), 170–183.

[7] Liu, W., Xie, W., Liu, J., and Wang, Y.
Adaptive double subspace signal detection in Gaussian background.
Part I: Homogeneous environments. IEEE Transactions on Signal Processing, **62**, 9 (Sep. 2014), 2345–2357.

[8] Liu, W., Xie, W., Liu, J., and Wang, Y.
Adaptive double subspace signal detection in Gaussian background.
Part II: Partially homogeneous environments. IEEE Transactions on Signal Processing, **62**, 9 (Sep. 2014), 2358–2369.

[9] Blunt, S. D., and Gerlach, K.
Efficient robust AMF using the FRACTA algorithm.
IEEE Transactions on Aerospace and Electronic Systems, **41**, 2 (Apr. 2005), 537–548.

[10] Gerlach, K. R., Blunt, S. D., and Picciolo, M. L.
Robust adaptive matched filtering using the FRACTA algorithm.
IEEE Transactions on Aerospace and Electronic Systems, **40**, 3 (Jul. 2004), 929–945.

[11] De Maio, A., Kay, S. M., and Farina, A.
On the invariance, coincidence, and statistical equivalence of the GLRT, Rao test, and Wald test.
IEEE Transactions on Signal Processing, **58**, 4 (Apr. 2010), 1967–1979.

[12] Orlando, D., and Ricci, G.
A Rao test with enhanced selectivity properties in homogeneous scenarios.
IEEE Transactions on Signal Processing, **58**, 10 (Oct. 2010), 5385–5390.

[13] Greco, M., Gini, F., and Diani, M.
Robust CFAR detection of random signals in compound-Gaussian clutter plus thermal noise.
IEE Proceedings Radar Sonar and Navigation, **148**, 4 (Aug. 2001), 227–232.

[14] He, Y., Jian, T., Su, F., Qu, C., and Gu, X.
Novel range-spread target detectors in non-Gaussian clutter.
IEEE Transactions on Aerospace and Electronic Systems, **46**, 3 (Jul. 2010), 1312–1328.

[15] Liu, J., Li, H., and Himed, B.
A CFAR adaptive subspace detector for first-order or second-order Gaussian signals based on a single observation.
IEEE Transactions on Signal Processing, **59**, 11 (Nov. 2011), 5126–5140.

[16] Liu, J., Li, H., and Himed, B.
Threshold setting for adaptive matched filter and adaptive coherence estimator.
IEEE Signal Processing Letters, **22**, 1 (Jan. 2015), 11–15.

[17] De Maio, A., and Orlando, D.
An invariant approach to adaptive radar detection under covariance persymmetry.
IEEE Transactions on Signal Processing, **63**, 5 (Mar. 2015), 1297–1309.

[18] De Maio, A., and Conte, E.
Adaptive detection in Gaussian interference with unknown covariance after reduction by invariance.
IEEE Transactions on Signal Processing, **58**, 6 (Jun. 2010), 2925–2934.

[19] Richards, M. A., Scheer, J. A., and Holm, W. A.
Principles of Modern Radar: Basic Principles. Edison, NJ: Scitech Publishing, Inc., 2010.

[20] Cann, A. J.
Range gate straddling loss and joint probability with partial correlation.
IEEE Transactions on Aerospace and Electronic Systems, **38** (Jul. 2002), 1054–1058.

[21] Zhang, X., Willett, P. K., and Bar-Shalom, Y.
Monopulse radar detection and localization of multiple unresolved targets via joint bin processing.
IEEE Transactions on Signal Processing, **53**, 4 (Apr. 2005), 1225–1236.

[22] Zhang, X., Willett, P.K., and Bar-Shalom, Y.
Detection and localization of multiple unresolved extended targets via monopulse radar signal processing.
IEEE Transactions on Aerospace and Electronic Systems, **45**, 2 (Apr. 2009), 455–472.

[23] Orlando, D., and Ricci, G.
Adaptive radar detection and localization of a point-like target.
IEEE Transactions on Signal Processing, **59**, 9 (Sep. 2011), 4086–4096.

[24] Ward, J.
Space-time adaptive processing for airborne radar.
MIT, Lexington, MA, Technical Report 1015, Dec. 13, 1994.

[25] Hao, C., Gazor, S., Foglia, G., Liu, B., and Hou, C.
Persymmetric adaptive detection and range estimation of a point-like target.
IEEE Transactions on Aerospace and Electronic Systems, **51**, 1 (Oct. 2015), 2590–2604.

[26] Nitzberg, R.
Application of maximum likelihood estimation of persymmetric covariance matrices to adaptive processing.
IEEE Transactions on Aerospace and Electronic Systems, **16**, 1 (Jan. 1980), 124–127.

[27] Conte, E., and De Maio, A.
Exploiting persymmetry for CFAR detection in compound-Gaussian clutter.
IEEE Transactions on Aerospace and Electronic Systems, **39**, 2 (Apr. 2003), 719–724.

[28] Giuli, D.
Polarization diversity in radars.
Proceedings of the IEEE, **74**, 2 (Feb. 1986), 245–269.

[29] Park, H., Li, J., and Wang, H.
Polarization space time domain generalized likelihood ratio detection of radar targets.
Signal Process, **41**, 2 (Jan. 1995), 153–164.

[30] De Maio, A., and Ricci, G.
A polarimetric adaptive matched filter.
Signal Process, **81**, 12 (Dec. 2001), 2583–2589.

[31] Pastina, D., Lombardo, P., and Bucciarelli, T.
Adaptive polarimetric target detection with coherent radar. I. Detection against Gaussian background.
IEEE Transactions on Aerospace and Electronic Systems, **37**, 4 (Oct. 2001), 1194–1206.

[32] Lombardo, P., Pastina, D., and Bucciarelli, T.
Adaptive polarimetric target detection with coherent radar. II. Detection against non-Gaussian background.
IEEE Transactions on Aerospace and Electronic Systems, **37**, 4 (Oct. 2001), 1207–1220.

[33] De Maio, A., and Alfano, G.
Polarimetric adaptive detection in non-Gaussian noise.
Signal Process, **83**, 2 (Feb. 2003), 297–306.

[34] De Maio, A., Alfano, G., and Conte, E.
Polarization diversity detection in compound-Gaussian clutter.
IEEE Transactions on Aerospace and Electronic Systems, **40**, 1 (Jan. 2004), 114–131.

[35] Alfano, G., De Maio, A., and Conte, E.
Polarization diversity detection of distributed target in compound-Gaussian clutter.
IEE Transactions on Aerospace and Electronic Systems, **40**, 2 (Apr. 2004), 755–765.

[36] Wang, J., and Nehorai, A.
Adaptive polarimetry design for a target in compound-Gaussian clutter.
Signal Processing, **89**, 6 (Jun. 2009), 1061–1069.

[37] Kong, L., Cui, G., Yang, X., and Yang, J.
Rao and Wald tests design of polarimetric multiple-input

multiple-output radar in compound-Gaussian clutter.
IET Signal Processing, **5**, 1 (Feb. 2011), 85–96.

[38] Cui, G., Kong, L., Yang, X., and Yang, J.
Distributed target detection with polarimetric MIMO radar in compound-Gaussian clutter.
Digital Signal Processing, **22**, 3 (May 2012), 430–438.

[39] De Maio, A.
Polarimetric adaptive detection of range-distributed targets.
IEEE Transactions on Signal Processing, **50**, 9 (Sep. 2002), 2152–2159.

[40] Garren, D. A., Odom, A. C., Pillai, S. U., and Guerci, J. R.
Full polarization matched illumination for target detection and identification.
IEEE Transactions on Aerospace and Electronic Systems, **38**, 2 (Jul. 2002), 824–837.

[41] Novak, L. M., Sechtin, M. B., and Cardullo, M. J.
Studies of target detection algorithms that use polarimetric radar data.
IEEE Transactions on Aerospace and Electronic Systems, **25**, 2 (Mar. 1989), 150–165.

[42] Novak, L. M., Burl, M. C., and Irving, W. W.
Optimal polarimetric processing for enhanced target detection.
IEEE Transactions on Aerospace and Electronic Systems, **29**, 1 (Jan. 1993). 234–244.

[43] Hurtado, M., and Nehorai, A.
Polarimetric detection of targets in heavy inhomogeneous clutter.
IEEE Transactions on Signal Processing, **56**, 4 (Apr. 2008), 1349–1361.

[44] Bandiera, F., Orlando, D., and Ricci, G.
Advanced radar detection schemes under mismatched signal models.
Synthesis Lectures on Signal Processing, No. 8. San Rafael, CA: Morgan & Claypool Publishers, 2009.

[45] Ghobadzadeh, A., Gazor, S., Taban, M. R., Tadaion, A. A., and Moshtaghioun, S. M.
Invariance and optimality of CFAR detectors in binary composite hypothesis tests.
IEEE Transactions on Signal Processing, **62**, 14 (Jul. 2014), 3523–3535.

[46] Ghobadzadeh, A., Gazor, S., Taban, M. R., Tadaion, A. A., and Gazor, M.
Separating function estimation tests: A new perspective on binary composite hypothesis testing.
IEEE Transactions on Signal Processing, **60**, 11 (Nov. 2012), 5626–5639.

[47] Van Trees, H. L. *Detection, Estimation, and Modulation Theory*, Part I. New York, NY: Wiley, 2001.

[48] Anderson, T. W. *An Introduction to Multivariate Statistical Analysis*, 3rd ed. New York, NY: Wiley, 2003.

[49] Kay, S. M. *Fundamentals of Statistical Signal Processing, Detection Theory*. Vol. II. Upper Saddle River, NJ: Prentice Hall, 1998.

[50] Golub, G. H., and Van Loan, C. F. *Matrix Computations*, 2nd ed. Baltimore, MD: Johns Hopkins Univ. Press, 1989.

[51] The McMaster IPIX radar sea clutter database.
http://soma.ece.mcmaster.ca/ipix/.

[52] De Maio, A., Foglia, G., Conte, E., and Farina, A.
CFAR behavior of adaptive detectors: An experimental analysis.
IEEE Transactions on Aerospace and Electronics Systems, **41**, 1 (Jan. 2005), 233–251.

[53] Gini, F., Greco, M. V., Diani, M., and Verrazzani, L.
Performance analysis of two adaptive radar detectors against non-Gaussian real sea clutter data.
IEEE Transactions on Aerospace and Electronic Systems, **36**, 4 (Oct. 2000), 1429–1439.

[54] Blum, R. S., and McDonald, K. F.
Analysis of STAP algorithms for cases with mismatched steering and clutter statistics.
IEEE Transactions on Signal Processing, **48**, 2 (Feb. 2000), 301–310.

[55] Richmond, C. D.
Performance of a class of adaptive detection algorithms in nonhomogeneous environments.
IEEE Transactions on Signal Processing, **48**, 5 (May 2000), 1248–1262.

[56] Bandiera, F., and Ricci, G.
Adaptive detection and interference rejection of multiple point-like radar targets.
IEEE Transactions on Signal Processing, **54**, 12 (Dec. 2006), 4510–4518.

[57] Sangston, K. J., Gini, F., and Greco, M. S.
Coherent radar target detection in heavy-tailed compound-Gaussian clutter.
IEEE Transactions on Aerospace and Electronic Systems, **48**, 1 (Jan. 2012), 64–77.

[58] Watts, S.
Radar detection prediction in K-distributed sea clutter and thermal noise.
IEEE Transactions on Aerospace and Electronic Systems, **23**, 1 (Jan. 1987), 40–45.

[59] Rangaswamy, M.
Statistical analysis of the nonhomogeneity detector for non-Gaussian interference backgrounds.
IEEE Transactions on Signal Processing, **53**, 6 (Jun. 2005), 2101–2111.

[60] Tylavsky, D. J., and Sohie, G. R. L.
Generalization of the matrix inversion lemma.
Proceedings of the IEEE, **74**, 7 (Jul. 1986), 1050–1052.

Chengpeng Hao (M'08-SM'15) received the B.S. and M.S. degrees in electronic engineering from Beijing Broadcasting Institute, Beijing, China, in 1998 and 2001 respectively. He received the Ph.D. degree in signal and information processing from Institute of Acoustics, Chinese Academy of Sciences, Beijing, China, in 2004. He is currently a professor of the State Key Laboratory of Information Technology for Autonomous Underwater Vehicles, Chinese Academy of Sciences. His research interests are in the field of statistical signal processing with more emphasis on adaptive sonar and radar signal processing. He has held a visiting position with the Electrical and Computer Engineering Department, Queens University, Kingston, Canada (July 2013–July 2014). He is now serving as a guest editor for the EURASIP Journal on Advances in Signal Processing for the issue on Advanced Techniques for Radar Signal Processing.

Saeed Gazor (S'94-M'95-SM'98) received the B.Sc. degree in electronics engineering in 1987 and the M.Sc. degree in communication systems engineering in 1989 from Isfahan University of Technology. He received the Ph.D. degree in signal and image processing from Telecom Paris, Departement Signal (cole Nationale Superieure des Tlecommunications/ENST, Paris), France, in 1994. Since 1999, he has been on the Faculty at Queen's University at Kingston, Ontario, Canada, and currently holds the position of full professor at the Department of Electrical and Computer Engineering and is also cross-appointed to the Department of Mathematics and Statistics at Queen's University. His main research interests are statistical and adaptive signal processing, detection and estimation theory, cognitive signal processing, array signal processing, speech processing, and information theory. Dr. Gazor's research has earned him a number of awards including a Provincial Premier's Research Excellence Award, a Canadian Foundation of Innovation Award, an Ontario Innovation Trust Award, and an Intel Research Excellence Award. He is a member of Professional Engineers Ontario. He has been on the technical program committee of numerous conferences and has served as an organizing committee member of many international conferences in various capacities, such as publication chair for the 11th IEEE ISSPA 2012 in Montreal and 26th BSC 2012 in Kingston, technical program (co-)chair for the IEEE WoSPA 2011 in Algeria, 24th BSC 2008 in Ontario, and the 11th IEEE ISSPA 2012. He was also the special sessions chair for ISSPA 2012. He served as a guest editor for the IEEE Journal on Selected Areas in Communications for the issue on theories and methods for advanced wireless relays. he is currently serving as associate editor for the IEEE Signal Processing Letters.

Xiaochuan Ma received the B.Sc. and M.Sc. degrees in automatic control and Ph.D. degree in electrical engineering from Northwestern Polytechnical University, Xian, China, in 1991, 1994, and 1997, respectively. From 1997 to 1999, he was a postdoctoral fellow with the Institute of Acoustics, Chinese Academy of Sciences (IACAS), Beijing, China. From 1999 to 2002, he worked with IBM China Research Center as a staff research member. He joined IACAS as a professor in 2003, and became a deputy director in 2009. His current research interests include underwater acoustics and signal processing. Dr. Ma is currently a board member of the Acoustical Society of China, as well as a member of the Signal Processing Technical Committee of Chinese Institute of Electronics.

Shefeng Yan (M'05-SM'10) received B.Sc., M.Sc., and Ph.D. degrees in electrical engineering from Northwestern Polytechnical University, Xi'an, China, in 1999, 2001, and 2005, respectively. He was a postdoctoral research associate with IACAS, Beijing, China, from 2005 to 2007, and with the Department of Electronics and Telecommunications, Norwegian University of Science and Technology, Trondheim, Norway, from 2007 to 2009. In 2009, he joined IACAS as a professor and was then appointed as the director of the Intelligent Sensing and Signal Processing Laboratory at IACAS. He is the author of the book Sensor Array Beampattern Optimization: Theory with Applications (Science Press, 2009). His current research interests include underwater acoustics, statistical and array signal processing, and their applications. Professor Yan is an outstanding young scholar of Hundred Talents Program with the Chinese Academy of Sciences. He is a recipient of the Chinese 2008 National Excellent Doctoral Dissertation Award, as well as a recipient of the 2010 International Commission on Acoustics-Acoustical Society of America Young Scientist Grant for excellent contributions to acoustics. He is also a corecipient of the Best Paper Awards at Sensor Technologies and Applications 2008 and Workshop on Applications of Signal Processing to Audio and Acoustics 2009.

Chaohuan Hou (SM'96-F'01) received the B.Sc. degree in physics from Peking University, Beijing, China, in 1958. Since 1958, he has worked on underwater acoustics and signal processing with the IACAS, Beijing, where he became a professor in 1985. He was the deputy director of IACAS from 1993 to 1997. He has published more than 200 journal and conference papers. His current research interests are in underwater acoustics, digital signal processing, arrays signal processing, very-large-scale integration signal processing, and application-specific integrated circuit chip design. Professor Hou was elected as an academician of the Chinese Academy of Sciences in 1995. He was the president of the Acoustical Society of China from 2002 to 2006 and then became the honorary president. From 2007 to 2010, he was a board member of the International Commission for Acoustics.

Danilo Orlando (SM'13) was born in Gagliano del Capo, Italy, on August 9, 1978. He received the Dr. Eng. degree (with honors) in computer engineering and the Ph.D. degree (with maximum score) in information engineering, both from the University of Salento (formerly University of Lecce), Italy, in 2004 and 2008, respectively. From July 2007 to July 2010, he has worked with the University of Cassino (Italy), engaged in a research project on algorithms for track-before-detect of multiple targets in uncertain scenarios. From September to November 2009, he has been visiting scientist at the NATO Undersea Research Centre (NURC), La Spezia, Italy, where he collaborated with Dr. F. Ehlers on track-before-detect strategies for multistatic sonars. From September 2011 to April 2015, he has worked at Elettronica SpA engaged as system analyst in the field of electronic warfare. In May 2015, he joined Universitá degli Studi "Niccoló Cusano," where he is currently associate professor. His main research interests are in the field of statistical signal processing and image processing with more emphasis on adaptive detection and tracking of multiple targets in multisensor scenarios. He has held visiting positions with the department of Avionics and Systems of ENSICA (now Institut Supérieur de l'Aéronautique et de l'Espace, ISAE), Toulouse, France, in February to March 2007, where he has worked with Professor O. Besson on adaptive radar detection in presence of mismatched signals. He is Senior Member of IEEE and author or coauthor of more than 50 scientific publications in international journals, conferences, and books. In 2015, he was appointed Senior Area Editor for IEEE Transactions on Signal Processing. Now he is serving as the lead guest editor for the EURASIP Journal on Advances in Signal Processing for the issue on Advanced Techniques for Radar Signal Processing.